

**New Observations of Extra-Disk Molecular Gas
in Interacting Galaxy Systems,
Including a Two-Component System in Stephan's Quintet**

Beverly J. Smith

Department of Physics and Astronomy, East Tennessee State University, Box 70652,
Johnson City TN 37604

Curtis Struck

Department of Physics and Astronomy, Iowa State University, Ames IA 50012

Received _____; accepted _____

ABSTRACT

We present new CO (1 – 0) observations of eleven extragalactic tails and bridges in nine interacting galaxy systems, almost doubling the number of such features with sensitive CO measurements. Eight of these eleven features were undetected in CO to very low CO/HI limits, with the most extreme case being the NGC 7714/5 bridge. This bridge contains luminous H II regions and has a very high HI column density ($1.6 \times 10^{21} \text{ cm}^{-2}$ in the $55''$ CO beam), yet was undetected in CO to rms $T_R^* = 2.4 \text{ mK}$. The HI column density is higher than standard H₂ and CO self-shielding limits for solar-metallicity gas, suggesting that the gas in this bridge is metal-poor and has an enhanced N_{H_2}/I_{CO} ratio compared to the Galactic value. Only one of the eleven features in our sample was unambiguously detected in CO, a luminous HI-rich star formation region near an optical tail in the compact group Stephan’s Quintet. We detect CO at two widely separated velocities in this feature, at $\sim 6000 \text{ km s}^{-1}$ and $\sim 6700 \text{ km s}^{-1}$. Both of these components have HI and H α counterparts. These velocities correspond to those of galaxies in the group, suggesting that this gas is material that has been removed from two galaxies in the group. The CO/HI/H α ratios for both components are similar to global values for spiral galaxies.

Subject headings: Galaxies: Individual (Stephan’s Quintet, NGC 7714/5) – Galaxies: ISM – Galaxies: Interactions

1. Introduction

Large amounts of interstellar gas can be removed from the main disks of spiral galaxies by four main processes: tides due to the gravitational force of a companion, ram pressure stripping during a near-head-on collision between gas-rich galaxies, ram pressure stripping by intracluster gas, and galactic winds driven by supernovae. By ejecting processed gas into intergalactic space, these mechanisms contribute to the metal-enrichment of the intergalactic medium. In many cases, which of these four processes is active in a given galaxy system can be determined from the optical, radio, and/or X-ray morphology. The signature of a tidal encounter between two galaxies is the presence of long stellar and/or HI tails and bridges (e.g., Toomre & Toomre 1972), while head-on collisions between gas-rich galaxies can produce ring galaxies (e.g., Lynds & Toomre 1976; Theys & Spiegel 1977) as well as gaseous bridges between the galaxies (Struck 1997). Ram pressure stripping by intracluster gas leads to an HI deficiency (e.g., Giovanelli & Haynes 1983), truncation of the outer HI disk of a galaxy (Cayette et al. 1990), and in some cases, bending of the HI disk (Kenney & Koopmann 1999), but not usually removal of large quantities of molecular gas (Kenney & Young 1989). Galactic winds are identified by extended extra-disk ionized gas without stellar counterparts (e.g., Rand, Kulkarni, & Hester 1990).

Star formation sometimes occurs in gas clouds far removed from the main disks of galaxies. Of the four processes that can remove gas from disks, the best-known to trigger the formation of young stars in the stripped gas is tidal forces: numerous examples of luminous H II regions in tidal features have been found (e.g., Schweizer 1978; Mirabel et al. 1991, 1992). Young stars have also been found in extra-disk gas clouds thought to have been stripped during head-on collisions (Smith et al. 1999) and interstellar-intracluster encounters (Xu et al. 1999).

In order to better understand the processes that lead to the removal of gas from

galaxies and the triggering of star formation in this gas, it is important to make a complete inventory of the gas in these features. This means not just the atomic gas, which has been surveyed in a large number of extragalactic tails and bridges (e.g., Haynes et al. 1984; Smith 1991; Hibbard & van Gorkom 1996), but also the molecular gas. Molecular gas has proved elusive in classical tidal tails; in our earlier CO survey of six tidal tails (Smith & Higdon 1994), no CO was found to very low levels, while only very low mass concentrations of molecular gas ($\leq 10^7 M_\odot$) were found in the tidal features of the nearby interacting system M81/M82/NGC 3077 (Brouillet, Henkel, & Baudry 1992; Walter & Heithausen 1999).

In contrast to tidal features, gas removed from galaxy disks by ram pressure during head-on collisions between two gas-rich galaxies may be richer in CO. The proto-type of this class of object is the CO-rich gas concentration found outside the disk of the Virgo Cluster galaxy NGC 4438 by Combes et al. (1988). If the standard Galactic N_{H_2}/I_{CO} ratio holds in this feature, it contains $M_{H_2} \sim 10^9 M_\odot$. The ring-like morphology of NGC 4438 and the proximity of the companion galaxy NGC 4435 suggests that this clump was removed during a head-on collision between the two galaxies (Kenney et al. 1995). Another apparent example of gas ram pressure-stripped during a galaxy-galaxy collision is the eastern tail of the peculiar galaxy NGC 2782. This feature has strong CO emission, corresponding to $6 \times 10^8 M_\odot$, assuming the Galactic N_{H_2}/I_{CO} conversion factor (Smith et al. 1999). Based on morphological considerations, we surmised that this feature was created during a near head-on collision between two galaxies, rather than a grazing encounter (Smith 1994).

These results suggest that features produced in head-on collisions may differ in a fundamental way from classical tidal tails and bridges formed during grazing encounters: they may be richer in CO. During a head-on collision, the material pulled out into a tail or bridge may originate in the inner disk of one of the galaxies, and so may be more metal-rich than gas pulled out from the outer disk in a more distant encounter. The metallicity of

the gas may affect the N_{H_2}/I_{CO} ratio, and therefore the detectability of the CO line. Both theoretical (e.g., Maloney & Black 1988) and observational (e.g., Wilson 1995; Verter & Hodge 1995; Arimoto, Sofue, & Tsujimoto 1996) studies show that low metallicities can lead to enhanced N_{H_2}/I_{CO} ratios compared to the Galactic value. In gas with low abundances and dust content, ultraviolet radiation penetrates more deeply into a molecular cloud, causing a larger C^+ region relative to the CO core, increasing the N_{H_2}/I_{CO} ratio.

The conclusion that tidal gas differs from ram pressure stripped gas is quite uncertain, in part because of the very small sample size. We have therefore continued our CO survey of extragalactic tails and bridges, selecting systems with high HI column densities, strong star formation rates, and/or ring-like morphologies. In this paper, we present new CO data for tails and bridges in nine additional interacting galaxy systems. We compare these data with the previous results discussed above, as well as the new CO data discussed in Smith (2000), Braine et al. (2000), and Gao et al. (2000).

Throughout this paper, we assume $H_o = 75 \text{ km s}^{-1} \text{ Mpc}^{-1}$.

2. Observations

The CO (1 – 0) observations were made using the 3mm SIS receiver on the National Radio Astronomy Observatory¹ (NRAO) 12m telescope during several observing runs between 1996 and 2000. Two 256×2 MHz filterbanks, one for each polarization, were used for the observations, providing a total bandpass of 1300 km s^{-1} with a spectral resolution of 5.2 km s^{-1} . A nutating subreflector with an azimuthal beam throw of $3'$ was used, taking care to avoid chopping on other galaxies, tails, or bridges in the system. Each

¹The National Radio Astronomy Observatory is a facility of the National Science Foundation, operated under cooperative agreement by Associated Universities, Inc.

scan was 6 minutes long. The beamsize FWHM is $55''$ at 115 GHz. The pointing was checked periodically with bright continuum sources and was consistent to $10''$. The system temperatures ranged from 200 to 500 K. Calibration was accomplished using an ambient chopper wheel.

A total of 45 positions in nine interacting systems were observed. These nine systems are listed in Table 1, along with a brief description of their optical morphologies. In Figure 1, we display optical images of these systems, obtained from the Digitized Sky Survey² (DSS). Table 2 lists the observed positions in the galaxies and tails/bridges; these positions and the CO FWHM beamwidth are marked in Figure 1. Fourteen of the observed positions were in tails or bridges; the rest were in the main disks of the galaxies. A total of eleven tails and bridges were observed. In three systems (Arp 144, NGC 2814/20, and NGC 3628), we observed multiple positions in a single tail or bridge.

Table 2 also lists the central velocities of the observed bandpasses. Note that I Zw 192, NGC 3561B, and position A in Stephan’s Quintet were all observed twice, with two different central velocities, to increase the observed bandpass; these two sets of data were combined.

The results of the CO observations are given in Table 3: the line fluxes, velocities, widths, and rms noise levels. The summed spectra for each observed position are displayed

²The Digitized Sky Survey was produced at the Space Telescope Science Institute under U.S. Government grant NAG W-2166. These images are digitized versions of photographic plates from the Second Palomar Observatory Sky Survey (POSS-II) made by the California Institute of Technology with funds from the National Science Foundation, the National Geographic Society, the Sloan Foundation, the Samuel Oshin Foundation, and the Eastman Kodak Corporation.

in Figure 2. Note that the center of NGC 7828 and one of the tail positions in this system were previously observed by Smith & Higdon (1994); the new and old data have been combined.

3. Results

Out of our nine interacting systems, the only unambiguous detection of CO outside of the main disk of a galaxy is the star formation region in Stephan’s Quintet. In two of our systems (NGC 3395/6 and the Taffy Galaxies), the two galaxies in the pair are separated by only $70'' - 90''$, and the star formation regions in the bridges are unresolved from the main disks with our beamsize. Thus, although the bridge positions were detected in CO, this may be emission from the galaxy disk in the 12m beam. Higher resolution follow-up observations are needed to confirm the existence of CO in these regions.

In Table 4, we give the molecular gas mass for the galaxy disks, derived assuming the standard Galactic N_{H_2}/I_{CO} ratio ($2.8 \times 10^{20} \text{ cm}^{-2}/(\text{K km s}^{-1})$; Bloemen et al. 1986) and the emission fills the beam ($\eta_c = 0.82$). For the galaxies where more than one position in the disk was detected, the total CO flux from the galaxy was obtained assuming a Gaussian distribution. For the observed extra-disk positions in these systems, the molecular gas mass was derived under the same assumptions, and are recorded in Table 5. Although these assumptions may not hold in all cases, they provide a basis for comparison. In Table 5, we also provide the HI column densities averaged over the CO beam, along with the implied M_{H_2}/M_{HI} ratios and the beam size Θ , in kpc.

For comparison, in Table 6, we give results for thirteen other tails, bridges, and extra-disk gas clouds previously observed in CO. This includes structures in NGC 2782 (Smith & Higdon 1994; Smith et al. 1999), NGC 4438 (Combes et al. 1988), NGC 4676,

NGC 7252, and Arp 143 (Smith & Higdon 1994), Arp 245 (Braine et al. 2000), NGC 4410 (Smith 2000), NGC 3561 (Braine et al. 2000), M81 (Brouillet et al. 1992) and NGC 3077 (Walter & Heithausen 1999), as well as the tentative (4σ) detection of CO in the southern tail of NGC 4038/9 (Gao et al. 2000). Note that in this paper we present CO data for the northern tail in the NGC 3561 system, while data for the southern feature are available from Braine et al. (2000). In Tables 5 and 6, we also give the $H\alpha$ luminosities for these sources, when available, as well as the $L_{H\alpha}/M_{H_2}$ ratio.

For the sources in Tables 5 and 6 which have HI data available, in Figure 3 we plot the HI column density in the CO beam N_{HI} against M_{H_2}/M_{HI} . For those with $H\alpha$ fluxes also available, in Figure 4 we compare $L_{H\alpha}/M_{H_2}$ with M_{H_2}/M_{HI} . Figures 3 and 4 show a wide range in $L_{H\alpha}/M_{H_2}$ and M_{H_2}/M_{HI} ratios for the features in our sample. The most extreme cases are 1) the NGC 7714/5 bridge, with a very high HI column density but very low CO flux, 2) the eastern feature of NGC 2782, with a low $L_{H\alpha}/M_{H_2}$ ratio, 3) the molecular clump near NGC 4438, with a very high implied M_{H_2}/M_{HI} ratio and a low $L_{H\alpha}/M_{H_2}$ value, and 4) the extra-disk star formation region in Stephan’s Quintet, with a high $L_{H\alpha}/M_{H_2}$ ratio.

The global ratios for spiral galaxies are typically $L_{H\alpha}/M_{H_2} \sim 0.0025 - 0.1 L_{\odot}/M_{\odot}$ and $M_{H_2}/M_{HI} \sim 0.2 - 6$ (Young et al. 1996). The star formation region in Stephan’s Quintet, the Arp 245 feature, the NGC 4038/9 paper, and the upper limits to the NGC 4676 tail and the NGC 3561 features are consistent with these global ratios. In contrast, the features in NGC 2782 and NGC 4438 have very low $L_{H\alpha}/M_{H_2}$ ratios, and the NGC 7714/5 bridge has a low implied M_{H_2}/M_{HI} ratio compared to global values for spirals.

Dwarf galaxies typically have higher $L_{H\alpha}/M_{H_2}$ ratios and lower M_{H_2}/M_{HI} ratios than normal spirals, if the standard Galactic conversion factor is applied. For example, the 14 dwarf galaxies in the Sage et al. (1992) sample have $L_{H\alpha}/M_{H_2} \geq 0.04 L_{\odot}/M_{\odot}$ and $M_{H_2}/M_{HI} \leq 0.5$, after converting to the standard Galactic conversion factor, while all but

two of the 25 dwarf galaxies studied by Israel, Tacconi, & Baas (1995) have M_{H_2}/M_{HI} ratios ≤ 0.02 with this conversion factor. The inferred molecular gas masses for dwarf galaxies may be low because their N_{H_2}/I_{CO} ratio is enhanced due to low metallicities (Maloney & Black 1988). Note, however, that specific locations within dwarf galaxies may have high implied M_{H_2}/M_{HI} ratios; for example, in IC 10, at positions with $N_H \geq 2 \times 10^{21} \text{ cm}^{-2}$, $M_{H_2}/M_{HI} \sim 3$ (Ohta, Sasaki, & Saito 1988).

The tails and bridges in Figure 3 that are undetected in CO have upper limits to their M_{H_2}/M_{HI} ratios consistent with global values for dwarfs. The upper limits for the NGC 3561 irregular, the NGC 7714 loop, the NGC 7715 tail, and the NGC 7714/5 bridge, are lower than typical global values for spirals; the rest have less strict upper limits.

The subset of these undetected features with $H\alpha$ fluxes available (NGC 4676, NGC 7714/5, and the northern tail of NGC 3561) have $L_{H\alpha}/M_{H_2}$ lower limits consistent with values for both dwarfs and spirals. However, the Arp 245 feature, the Stephan’s Quintet source, the NGC 4038/9 tail, the eastern NGC 2782 tail, and the NGC 4438 CO clump are brighter in CO relative to $H\alpha$ than typical dwarf galaxies, while Stephan’s Quintet, the eastern NGC 2782 tail, and the NGC 4438 CO clump have higher inferred M_{H_2}/M_{HI} ratios than dwarfs. The southern NGC 3561 feature has an M_{H_2}/M_{HI} ratio higher than that usually found in dwarfs, but just a lower limit to $L_{H\alpha}/M_{H_2}$.

4. Comments on Individual Galaxies

4.1. NGC 7714/5

The most extreme feature in our sample in terms of inferred M_{H_2}/M_{HI} ratio is the bridge of NGC 7714/5. This bridge, which contains luminous H II regions (Arp 1966; Bernlöhr 1993; González-Delgado et al. 1995; Smith et al. 1997), was not detected in CO,

in spite of its high column density of atomic hydrogen ($1.6 \times 10^{21} \text{ cm}^{-2}$ in the CO beam; from the data in Smith et al. 1997). At this bridge, our upper limit implies $N_{H_2} \leq 5.0 \times 10^{19} \text{ cm}^{-2}$ and $M_{H_2}/M_{HI} \leq 0.063$, more than three times smaller than our upper limit for the system with the second lowest M_{H_2}/M_{HI} ratio in a tail or bridge, the NGC 3561 irregular. The HI column density in this bridge is above the H_2 and CO self-shielding limits for solar metallicity gas ($\sim 5 \times 10^{20} \text{ cm}^{-2}$ and 10^{21} cm^{-2} , respectively; Federman et al. 1979; van Dishoeck & Black 1988). However, the nucleus of NGC 7714 is known to be low metallicity (French 1980; García-Vargas et al. 1997), so it is likely that the gas in the bridge would also have low abundances, leading to an enhanced N_{H_2}/I_{CO} ratio. Thus there may be more molecular gas in this system than implied by the CO measurements. We note that the mid-infrared camera on the Infrared Space Observatory (ISOCAM) did not detect this bridge (O’Halloran et al. 2000), but it did detect the more distant extra-disk source in Stephan’s Quintet (Xu et al. 1999). This suggests a smaller warm dust component in the NGC 7714/5 bridge.

The smaller galaxy NGC 7715, the eastern tail of NGC 7715, and the HI loop north of NGC 7714 are also weak in CO, with inferred M_{H_2}/M_{HI} ratios ≤ 0.16 , ≤ 0.16 , and ≤ 0.24 , respectively. These may also have enhanced N_{H_2}/I_{CO} ratios. Note that NGC 7715, its tail, and the NGC 7714 loop have not been detected in $H\alpha$ (Smith et al. 1997). Also note that NGC 7714 and NGC 7715 have absolute blue magnitudes of -19.8 and -18.1 , respectively (de Vaucouleurs et al. 1991), compared to -17.7 for the Large Magellanic Cloud (de Vaucouleurs et al. 1991; Sandage, Bell, & Tripicco 1999). At absolute magnitudes fainter than about -19 , both irregular and spiral galaxies typically have less than solar metallicities (Skillman et al. 1989; Vila-Costas & Edmunds 1992; Storch-Bergmann et al. 1994), thus NGC 7715 may also be metal-poor.

4.2. NGC 2782 and NGC 4438

At the other extreme from the NGC 7714/5 bridge in terms of CO brightness is the eastern tail of NGC 2782 and the extra-disk gas cloud near NGC 4438, with low $L_{H\alpha}/M_{H_2}$ ratios compared to the other features (see Figure 4). These features have strong CO emission, but little on-going star formation (Combes et al. 1988; Kenney et al. 1995; Smith et al. 1999). None of the features in our new sample are as rich in CO as the NGC 2782 and NGC 4438 features. As discussed at length in Smith et al. (1999), the gas in these features may be metal-rich material removed from the interiors of their disks by near-head-on collisions, leading to high CO fluxes. Star formation may be inhibited in these features because of the collision (Smith et al. 1999). Gas clouds pushed out of a galactic disk by a high velocity collision may compress and then adiabatically expand, reducing their self-gravity. This may decrease the rate of star formation and therefore the $L_{H\alpha}/M_{H_2}$ ratio.

4.3. Arp 245, NGC 3561, and NGC 4038/9

In Figure 3 and Tables 5 and 6, the structure with the highest HI column density in the CO beam is the northern tail of the relatively nearby galaxy Arp 245, which has $N_{HI} = 2.3 \times 10^{21} \text{ cm}^{-2}$ averaged over the 3.5 kpc beam (Duc et al. 2000). As discussed in Duc et al. (2000), this feature is relatively gas-rich and CO-rich ($M_{H_2} \sim 1.5 \times 10^8 M_\odot$, $M_{HI} \sim 4.8 \times 10^8 M_\odot$, and $M_{H_2}/M_{HI} \sim 0.31$ in the CO beam) and has many properties in common with spiral galaxies. It has an $L_{H\alpha}/M_{H_2}$ ratio similar to spirals, and a stellar population dominated by an underlying old population (Duc et al. 2000). Furthermore, it has a relatively high extinction ($A_B = 2.6$, from the Balmer decrement), a high blue luminosity ($M_B = -17.2$ and $L_B = 1.2 \times 10^9 L_\odot$, uncorrected for internal extinction), and a metallicity of $12 + \log(O/H) \sim 8.6$ (Duc et al. 2000). With a modest correction for internal extinction, these values are consistent with the metallicity-luminosity relationship

for late-type spirals (Zaritsky, Kennicutt, & Huchra 1994; Garnett et al. 1997). Thus it is possible that this structure may not be a tidal tail, but rather a pre-existing edge-on disk galaxy that is interacting with the other two galaxies in the system. High resolution kinematic data may be useful in testing this hypothesis. In any case, this feature appears to be richer in CO relative to HI and H α than most dwarf galaxies.

The fact that the Arp 245 feature was detected in CO and many of the other features were not may be due to its high HI column density and relatively high metallicity. There is some evidence that N_{H_2}/I_{CO} is correlated with metallicity (Wilson 1995; Verter & Hodge 1995; Arimoto et al. 1996). The trends implied in these papers suggest that at the metallicity of the Arp 245 feature, the N_{H_2}/I_{CO} ratio is enhanced only slightly, between 1.5 – 3 times bigger than the Galactic value. Thus, at the high HI column density of the Arp 245 feature, the CO self-shielding limit is exceeded. We note that IC 10, which has a lower oxygen abundance than the Arp 245 feature, shows strong CO at positions where N_{HI} exceeds 10^{21} cm^{-2} (Ohta, Sasaki, & Saito 1988). At present, the metal abundances of most of the features listed in Tables 5 and 6 are unknown.

The NGC 3561 system (Arp 105; Figure 1d) contains a spiral (NGC 3561A), an S0 or E galaxy (NGC 3561B), and two tidal features with on-going star formation, presumably pulled out from the spiral galaxy. The concentration of gas and star formation in the northern tail is classified as a Magellanic irregular by Duc & Mirabel (1994). The southern feature, which crosses the companion NGC 3561B, is visible as an optical knot in Figure 1d, and is classified as a compact dwarf by Duc & Mirabel (1994). This southern feature was detected in CO by Braine et al. (2000), yielding a high M_{H_2}/M_{HI} ratio in the CO beam of ~ 0.8 . This ratio is higher than that of the Arp 245 feature, in spite of its more modest HI column density in the CO beam, $\sim 2 \times 10^{20} \text{ cm}^{-2}$ (Duc et al. 1997) and its lower oxygen abundance ($12 + \log(O/H) \sim 8.4$; Duc & Mirabel 1994). This feature also has a lower blue

luminosity ($M_B = -16.9$; $L_B = 9.0 \times 10^8 L_\odot$, uncorrected for internal extinction) and a lower extinction ($A_B = 1.0$) (Duc et al. 1994) than the Arp 245 feature.

The northern tail of NGC 3561 (the Magellanic irregular) has a peak HI column density four times higher and a blue luminosity five times larger than the southern tail (Duc et al. 1997), and has a higher oxygen abundance $12 + \log(\text{O}/\text{H}) \sim 8.6$ (Duc & Mirabel 1994), but was undetected in CO, with a lower M_{H_2}/M_{HI} ratio of ≤ 0.2 . This difference may be due in part to the difference in beam sizes of our CO observations and the higher resolution observations of Braine et al. (2000), which are less affected by beam dilution. In the interaction scenario for this system presented by Duc et al. (1997), the spiral galaxy NGC 3561A interacts with the elliptical NGC 3561B, drawing out a long tail to the north, and a shorter countertail to the south. Since both features may have originated in NGC 3561A, it is reasonable to expect they would have similar gas properties. The southern feature may have a relatively small angular size, high column density clump in which the self-shielding limits are exceeded.

If the tentative detection of CO in the NGC 4038/9 tail (Gao et al. 2000) is confirmed by more sensitive observations, it places this tail in the same category as the NGC 3561 and Arp 245 features: it is richer in CO than dwarf galaxies, relative to its $H\alpha$ flux. The metallicity in this feature has been estimated to be somewhat lower than that in the Arp 245 feature, $12 + \log(\text{O}/\text{H}) \sim 8.4$ (Mirabel et al. 1992).

4.4. M81 and NGC 3077

The tidal features of M81 and NGC 3077 have also been detected in CO (Brouillet et al. 1992; Walter & Heithausen 1999). Like those in Arp 245 and NGC 3561, they also have high inferred M_{H_2}/M_{HI} ratios (Table 6). However, the inferred H_2 masses in the CO beam

are small ($\sim 10^6 M_\odot$, using the standard Galactic N_{H_2}/I_{CO} ratio; $10^7 M_\odot$, using the virial theorem) and there is no evidence for on-going star formation in these locations (Brouillet et al. 1992; Henkel et al. 1993; Walter & Heithausen 1999). The M81/M82/NGC 3077 group is very nearby, so the area subtended by the CO beam (~ 360 pc) is much smaller than in the other systems listed. The other features plotted in Figure 3 have physical beam diameters ranging from 1.8 kpc (NGC 4438) to 43 kpc (I Zw 192). As with the Arp 245 and NGC 3561 features, the CO self-shielding threshold may be exceeded locally in these features. We note that the HI column density in the CO beam is quite high for the M81 and NGC 3077 positions, 10^{21} cm^{-2} .

A recent larger area CO survey of the NGC 3077 tail (Walters & Heithausen 2000) shows CO in two clumps covering an area of about $3'$ (2.8 kpc). In this region, the standard Galactic conversion factor gives $M_{H_2} \sim 6 \times 10^6 M_\odot$ and an average H_2 column density of $\sim 8 \times 10^{19} \text{ cm}^{-2}$. As in IC 10, CO is only detected at HI column densities above $\sim 10^{21} \text{ cm}^{-2}$. In this larger area, the inferred M_{H_2}/M_{HI} ratio is smaller, ~ 0.1 , consistent with the upper limits on the undetected tails and bridges in the sample.

4.5. Stephan’s Quintet

Of the nine extra-disk locations in our new sample, only one was detected in CO: the position in Stephan’s Quintet (HCG 92; Arp 319). Stephan’s Quintet is a compact group of four galaxies with similar velocities ($\sim 6000 \text{ km s}^{-1}$; NGC 7317, NGC 7318A/B, and NGC 7319), and a probable foreground galaxy (NGC 7320) with a much lower velocity ($\sim 800 \text{ km s}^{-1}$). The outlying galaxy NGC 7320C also has a velocity of $\sim 6000 \text{ km s}^{-1}$, and so probably also belongs to this group. Strong gravitational interactions are clearly present in this group (Figure 1g). A long optical tail stretches more than $1'$ (26 kpc) to the southeast of NGC 7319; this tail is also detected in HI (Shostak et al. 1984; Verdes-Montenegro et

al. 2000). Two more optical tails are seen extending to the north of the close pair NGC 7318A/B (see Figure 1g). Along the easternmost of these features, X-rays (Pietsch et al. 1997) and radio continuum emission (van der Hulst & Rots 1981) are visible, suggesting a shock front. At the location where the two optical tails of NGC 7318A/B intersect, a large concentration of ionized gas has been detected (Moles, Sulentic, & Márquez 1997; Ohyama et al. 1998; Xu et al. 1999). This source is also present in the optical DSS image (Figure 1g), in the mid-infrared map of Xu et al. (1999), and in HI (Shostak, Sullivan, & Allen 1984; Verdes-Montenegro et al. 2000). Optical spectroscopy shows that the ionization mechanism for this source is young stars, while spectral signatures of shocks are present to the south, along the radio continuum and X-ray ridge (Moles, Márquez, & Sulentic 1998).

At the location of the extra-disk star formation region in Stephan’s Quintet, we have detected two CO components, at 6000 km s^{-1} and 6700 km s^{-1} , at the 5σ and 6σ significance level, respectively. These two components have similar CO fluxes (Table 3). The large velocity separation of these two features argues against the idea that they are caused by the double-horned signature of a rotating disk, but are instead two distinct gas clouds. These two components each contain $1.0 \times 10^9 M_{\odot}$ of molecular gas, if the standard Galactic N_{H_2}/I_{CO} ratio holds. One of these components (6000 km s^{-1}) was detected at a 4σ level in the CO interferometer data of Gao & Xu (2000). We have also detected CO in NGC 7319 and NGC 7318B. NGC 7319 had previously been seen in CO (Verdes-Montenegro et al. 1998; Yun et al. 1997), however, the weaker CO flux from 7318B was not seen in those less sensitive studies. The CO detection in NGC 7318B is at 6000 km s^{-1} , a somewhat higher velocity than the optical velocity of this galaxy (5765 km s^{-1} ; Moles et al. 1998).

Both of the CO components in the extra-disk star formation region have HI counterparts (Shostak et al. 1984). They also both appear to have on-going star formation. Moles et al. (1998) obtained optical spectra of three H II regions in this vicinity; two have velocities of

$\sim 6020 \text{ km s}^{-1}$ and one has a velocity of 6680 km s^{-1} . Two $\text{H}\alpha$ velocity components are also indicated by the narrowband imaging of Xu et al. (1999).

The $\text{H}\alpha$ luminosity, molecular gas mass, and HI mass for the extra-disk source in Stephan’s Quintet are similar to those of many normal spiral galaxies (Young et al. 1996), but unlike those of typical dwarf galaxies (Sage et al. 1992). The implied $\text{M}_{\text{H}_2}/\text{M}_{\text{HI}}$ ratios for both velocity components in this region are very high, ~ 0.65 , higher than values typically found for dwarf galaxies (Sage et al. 1992). The $\text{L}_{\text{H}\alpha}/\text{M}_{\text{H}_2}$ ratio for the Stephan’s Quintet source, $0.016 \text{ L}_{\odot}/\text{M}_{\odot}$, is consistent with global values for spirals (Young et al. 1996), as well as the values found for the NGC 4676 tail, the Arp 245 feature, and the southern tail of NGC 3561, but is higher than the values seen for the eastern tail of NGC 2782 and the NGC 4438 clump. In Smith et al. (1999), we suggested that star formation was inhibited in the eastern tail of NGC 2782 and the NGC 4438 CO clump because of strong shocks sustained during a head-on collision between two gas-rich galaxies. If the extra-disk cloud in Stephan’s Quintet was formed in this way, star formation is clearly not inhibited.

To explain the peculiar morphology of Stephan’s Quintet, a number of different interaction scenarios have been suggested. Some of these scenarios involve ram pressure stripping during a head-on collision between two galaxies. For example, Peterson & Shostak (1980) suggest that a head-on collision between NGC 7318B and NGC 7319 removed the gas and caused the radio continuum ridge between them. A different scenario was suggested by Shostak et al. (1984): a prograde tidal encounter of NGC 7320C and NGC 7319 occurred, pulling gas out of these galaxies, creating the long tail south of NGC 7319. This was followed by a high-speed collision between NGC 7318A and NGC 7318B. Other scenarios involve a collision between an ‘intruder galaxy’ (usually NGC 7318B) and intragalactic gas that had previously been tidally-stripped or ram pressure-stripped in an earlier encounter

between two different galaxies in the group (van der Hulst & Rots 1981; Moles et al. 1997). Moles et al. (1997) suggest that a direct collision between the outlying galaxy NGC 7320C and NGC 7319 occurred in the recent past (10^8 years ago), removing a large quantity of gas from these galaxies. After this event, NGC 7318B entered the group at high velocity, colliding with this stripped gas and triggering star formation.

Our new data shed some light on the question of the origin of the extra-disk gas in Stephan’s Quintet. Our detection of two CO-rich components in the extra-disk star formation region shows that the star formation in this feature was triggered by a collision involving relatively high metallicity, molecule-rich gas concentrations, rather than metal-poor intracluster medium. This does not rule out ram pressure stripping of NGC 7318B by an intergalactic medium, but it does require that this intergalactic medium be relatively metal-rich gas: gas previously removed from a galaxy. How this gas was originally removed from the disk is unclear: as shown in Arp 245 and NGC 3561, structures apparently created by tidal forces can be relatively CO-rich. Thus this intergalactic gas may have been removed either by tidal forces, or via ram pressure stripping.

The 6700 km s^{-1} extra-disk component may have originally come from NGC 7319 or NGC 7318A, which have similar optical velocities (6650 km s^{-1} and 6620 km s^{-1} , respectively; Moles et al. 1998). The most likely candidate of these two is the barred spiral NGC 7319, which shows a surprising lack of H II regions (Arp 1973), a long optical tail, and a very offset CO distribution (Yun et al. 1997). NGC 7318A also has an optical tail, however, this may have been created by another interaction.

The 6000 km s^{-1} extra-disk gas may have originated in either the outlying galaxy NGC 7320C or in NGC 7318B. NGC 7320C has an optical radial velocity of $6000 \pm 150 \text{ km s}^{-1}$ (Lynds 1972), consistent with this velocity. Previous arguments for the involvement of NGC 7320C (Moles et al. 1997) cited the long tail south of NGC 7319 that points towards

NGC 7320C. Alternatively, this component of the extra-disk gas may have come from NGC 7318B. As noted above, our CO observations show a faint CO line in NGC 7318B at this velocity, redshifted 300 km s^{-1} from the optical velocity. This detection corresponds to a molecular gas mass of $1.7 \times 10^9 M_{\odot}$, assuming the standard N_{H_2}/I_{CO} conversion factor.

We therefore suggest that the extra-disk gas undergoing star formation in Stephan’s Quintet originated in NGC 7318B and NGC 7319. At the present time it is unclear whether a single collision between NGC 7318B and NGC 7319 occurred, ram pressure stripping the gas and creating the shock front between the two galaxies, or whether gas had been removed from NGC 7319 earlier, by an earlier encounter with another galaxy, and then this gas was impacted by NGC 7318B.

5. Conclusions

We have obtained new CO (1 – 0) observations of eleven extragalactic tails and bridges, and compared these measurements with previously-published data for another thirteen features. Of these 24 structures, four have inferred M_{H_2}/M_{HI} upper limits (assuming the Galactic N_{H_2}/I_{CO} conversion factor) less than global values for spiral galaxies, consistent with those found for irregular galaxies. Three of these four CO-poor features are in the NGC 7714/5 system; the most extreme case is the star forming bridge, which has a very high HI column density ($1.6 \times 10^{21} \text{ cm}^{-2}$ in the $55''$ CO beam), yet was undetected in CO, giving an inferred M_{H_2}/M_{HI} upper limit of ≤ 0.063 . These features may have enhanced N_{H_2}/I_{CO} ratios compared to the Galactic value due to low metallicities.

Of the 24 structures in our combined sample, eight have been detected in CO. Three of these eight (the Stephan’s Quintet extra-disk source, the NGC 4038/9 tail, and the Arp 245 tail) have inferred efficiencies of star formation ($L_{H\alpha}/M_{H_2}$) consistent with global

values for spiral galaxies. In contrast, the $L_{H\alpha}/M_{H_2}$ ratios for the eastern tail of NGC 2782 and the NGC 4438 clump are lower than typical for disk galaxies, suggesting inhibited star formation. In none of the features were our CO limits low enough to conclusively show $L_{H\alpha}/M_{H_2}$ ratios as high as those found in dwarf galaxies.

Of the eight detected features, two (NGC 2782 and NGC 4438) have optical morphologies indicating head-on collisions. The Stephan’s Quintet feature may also have been formed in this manner. In these systems, we suggest that metal-rich gas with an approximately Galactic N_{H_2}/I_{CO} ratio was pulled from the inner parts of the galaxies.

A few recent studies have reported the detection of CO in a number of classical tidal features (e.g., NGC 4038/9, Arp 245, and NGC 3561). In these structures, the HI column density may be locally high enough that the CO self-shielding limit is exceeded, in spite of modestly enhanced N_{H_2}/I_{CO} ratios. There is a slight tendency for these tidal features to have lower M_{H_2}/M_{HI} ratios and higher $L_{H\alpha}/M_{H_2}$ ratios than ram pressure stripped features discussed above, but there is a large amount of scatter and the sample size is small. More observations are needed to determine whether there is truly a statistical difference in the gaseous and star formation properties of tidal and ram pressure stripped features.

We are grateful for the help of the NRAO 12m telescope operators and staff in obtaining these data. This research has made use of the NASA/IPAC Extragalactic Database (NED) which is operated by the Jet Propulsion Laboratory under contract with NASA. We are pleased to acknowledge partial funding for this project from a NASA grant administrated by the American Astronomical Society and from NSF grant INT-9908542.

REFERENCES

- Arimoto, N., Sofue, Y., & Tsujimoto, T. 1996, PASJ, 48, 275
- Arp., H. C. 1966, Atlas of Peculiar Galaxies (Pasadena: California)
- Arp, H. 1973, ApJ, 183, 411
- Bernlöhr, K. 1993, A&A, 268, 25
- Bloemen, J. B., et al. 1986, A&A, 154, 25
- Bosma, A., Casini, C., Heidmann, J., van der Hulst, J. M., & van Woerden, H. 1980, A&A, 89, 345
- Bottinelli, L., Gouguenheim, L., Fouque, P., & Paturel, G. 1990, A&AS, 82, 391
- Braine, J., Lisenfield, U., Duc, P.-A., & Leon, S., 2000, Nature, 403, 867
- Brouillet, N., Henkel, C., & Baudry, A. 1992, A&A, 262, L5
- Cayette, V., van Gorkom, J. H., Balkowski, C., & Kotanyi, C. 1990, AJ, 100, 604
- Condon, J. J., Helou, G., Sanders, D. B., & Soifer, B. T. 1993, AJ, 105, 1730
- Combes, F., Dupraz, C., Casoli, F., & Pagani, L. 1988, A&A, 203, L9
- De Vaucouleurs, G., De Vaucouleurs, A., Corwin, Jr, Jr., H. G., Buta, R. J., Paturel, G., & Fouque, P. 1991, Third Reference Catalogue of Bright Galaxies, Version 3.9 (RC3)
- Duc., P.-A., Brinks, E., Springel, V., Pichardo, P., Wielbacher, P., & Mirabel, I. F. 2000, AJ, 120, 1238
- Duc., P.-A., Brinks, E., Winks, J. E., & Mirabel, I. F. 1997, A&A, 326, 537
- Duc, P.-A., & Mirabel, I. F. 1994, A&A, 289, 83
- Federman, S. R., Glassgold, A. E., & Kwan, J. 1979, ApJ, 227, 466
- French, H. B. 1980, ApJ, 240, 41

- Gao, Y., & Xu, C. 2000, ApJ, in press
- Gao, Y., Lo, K. Y., Lee, S.-W., and Lee, T.-H. 2000, ApJ, in press
- García-Vargas, M. L., González-Delgado, R. M., Pérez, E., Alloin, D., Díaz, A., & Terlevich, E. 1997, ApJ, 478, 112
- Garnett, D. R., Shields, G. A., Skillman, E. D., Sagan, S. P., & Dufour, R. J. 1997, ApJ, 489, 63
- Giovanelli, R., & Haynes, M. P. 1983, AJ, 88, 881
- González-Delgado, R. M., Pérez, E., Díaz, A. I., García-Vargas, M. L., Terlevich, E., & Vilchez, J. M. 1995, ApJ, 439
- Hibbard, J. E., van der Hulst, J. M., & Barnes, J. E. 2000, in preparation.
- Higdon, J. L. 1988, ApJ, 326, 146
- Huang, Z.-P., Yin, Q.-F., Saslaw, W. C., & Heeschen, D. S. 1994, ApJ, 423, 614
- Haynes, M. P., Giovanelli, R., & Chincarini, G. L. 1984, ARAA, 22, 445
- Henkel, C., Stickel, M., Salzer, J. J., Hopp, U., Brouillet, N., & Baudry, A. 1993, A&A, 273, L15
- Hibbard, J. E., & van Gorkom, J. H. 1996, AJ, 111, 655
- Higdon, J. L. 1988, ApJ, 326, 146
- Humphreys, R. M., & Aaronson, M. 1987, AJ, 94, 1156
- Israel, F. P., Tacconi, L. J., & Baas, F. 1995, A&A, 295, 599
- Kenney, J. D. P., & Koopmann, R. A. 1999, AJ, 117, 181
- Kenney, J. D. P., & Young, J. S. 1989, ApJ, 344, 171
- Kenney, J. D. P., Rubin, V. C., Planesas, P., & Young, J. S. 1995, ApJ, 438, 135
- Kormendy, J., & Bahcall, J. N. 1974, AJ, 79, 671

- Lynds, C. R. 1972, External Galaxies and Quasi-stellar Objects, IAU Symp. No. 44, Reidel, Dordrecht, p. 376
- Lynds, R., & Toomre, A. 1976, ApJ, 209, 382
- Maloney, P., & Black, J. H. 1988, ApJ, 325, 389
- Mirabel, I. F. et al. 1991, A&A, 243, 367
- Mirabel, I. F. et al. 1992, A&A, 256, L19
- Moles, M., Márquez, I., & Sulentic, J. W. 1998, A&A, 334, 473.
- Moles, M., Sulentic, J. W., & Márquez, I. 1997, ApJ, 485, L69
- O’Halloran, B., Metcalfe, L., Delaney, M., McBreen, B., Laureijs, R., Leech, K., Watson, D., & Hanlon, L. 2000, A&A, 360, 871
- Ohta, K., Sasaki, M., & Saito, M. 1988, PASJ, 40, 653
- Ohya, Y., Nishiura, S., Murayama, T., & Taniguchi, Y. 1998, ApJ, 492, L25
- Peterson, S. D., & Shostak, G. S. 1980, ApJ, 241, L1
- Pietsch, W., Trinchieri, G., Arp, H., & Sulentic, J. W. 1997, A&A, 322, 89
- Rand, R. J., Kulkarni, S. R., & Hester, J. J. 1990, ApJ, 352, L1
- Rots, A. H. 1978, AJ, 83, 219
- Rots, A. H., & Shane, W. W. 1975, A&A, 45, 25
- Sage, L. J., Salzer, J. J., Loose, H.-H., & Henkel, C. 1992, A&A, 265, 19
- Sandage, A., & Tammann, G. A. 1981, A Revised Shapley-Ames Catalog of Bright Galaxies (Washington: Carnegie Institution of Washington)
- Sandage, A., Bell, R. A., & Tripicco, M. J. 1999, ApJ, 522, 250
- Schweizer, F. in Structure and Properties of Nearby Galaxies, 1978, 279

- Shostak, G. S., Sullivan, W. T. III, & Allen, R. J. 1984, *A&A*, 139, 15
- Skillman, E. D., Kennicutt, R. C., & Hodge, P. W. 1989, *ApJ*, 347, 875
- Smith, B. J. 1989, Ph.D. Thesis, University of Massachusetts.
- Smith, B. J. 1991, *ApJ*, 378, 39
- Smith, B. J. 1994, *AJ*, 107, 1695
- Smith, B. J., & Higdon, J. L. 1994, *AJ*, 108, 837
- Smith, B. J., & Wallin, J. F. 1992, 393, 544
- Smith, B. J., Struck, C., & Pogge, R. W. 1997, *ApJ*, 483, 754
- Smith, B. J., Struck, C., Kenney, J. D. P., & Jogee, S. 1999, *AJ*, 117, 1237
- Smith, B. J. 2000, *ApJ*, 541, 624
- Storchi-Bergmann, T., Calzetti, D., & Kinney, A. L. 1994, *ApJ*, 429, 572
- Struck, C. 1997, *ApJS*, 113, 269
- Taylor, C. L., Kobulnicky, H. A., & Skillman, E. D. 1998, *AJ*, 116, 2746
- Theys, J. C., & Spiegel, E. A. 1977, *ApJ*, 212, 616
- Toomre, A., & Toomre, J. 1972, *ApJ*, 178, 623
- van der Hulst, J. M., & Hummel, E. 1985, *A&A*, 150, L7
- van der Hulst, J. M., & Rots, A. H. 1981, *AJ*, 86, 1775
- van Dishoeck, E. F., & Black, J. H. 1988, *ApJ*, 334, 771
- Verdes-Montenegro, L., Yun, M. S., Perea, J., del Olmo, A., & Ho, P. T. P. 1998, *ApJ*, 497, 89
- Verdes-Montenegro, L. 2000, in *Gas and Galaxy Evolution Conference Proceedings*, in press
- Verter, F., & Hodge, P. 1995, *ApJ*, 446, 616

- Vila-Costas, M. B., & Edmunds, M. G. 1992, MNRAS, 259, 121
- Walter, F., & Heithausen, A. 1999, ApJ, 519, L69
- Walter, F., & Heithausen, A. 2000, Proceedings of the Evolution of Galaxies on Cosmological Timescales Conference, ASP Conference Series, in press
- Wilson, C. D. 1995, ApJ, 448, L97
- Xu, C., Sulentic, J. W., & Tuffs, R. 1999, ApJ, 512, 178
- Young, J. S., Allen, L., Kenney, J. D. P., Lesser, A., & Rownd, B. 1996, AJ, 112, 1903
- Young, J. S., et al. 1995, ApJS, 98, 219
- Yun, M. S., Verdes-Montenegro, L., Del Olmo, A., & Perea, J. 1997, ApJ, 475, L21.
- Zaritsky, D., Kennicutt, R. C., Jr., & Huchra, J. P. 1994, ApJ, 420, 87

Captions

Figure 1. Optical images of the nine interacting galaxy systems in our sample, with the locations and FWHM beamsizes of the CO beams marked. All images are from the Digitized Sky Survey (DSS), except when noted. a) Arp 144 (NGC 7828/9). There is an HI tail without a known optical counterpart to the southeast of the optical pair (Higdon 1988). b) NGC 2814/20/MK 208. c) NGC 3395/6. d) Arp 105 (NGC 3561). This image has been smoothed by a $3''$ FWHM Gaussian to enhance low surface brightness features. e) The brightest galaxy in the Leo Triplet, NGC 3628. A long HI tail extends to the east of NGC 3628 (Rots 1978; Haynes, Giovanelli, & Roberts 1979); this tail has a faint optical counterpart not visible in the DSS image shown here (Kormendy & Bahcall 1974). The two marked locations are in this tail. We also observed the center of NGC 3628. f) I Zw 192. g) Stephan’s Quintet. h) A narrowband red continuum image of NGC 7714/5 (Arp 284), from Smith et al. (1997). i) UGC 12914/5 (Taffy Galaxies).

Figure 2. The summed CO ($1 - 0$) scans for the observed positions, after the spectra have been smoothed by a 36 km s^{-1} boxcar and then resampled at 21 km s^{-1} spacing.

Figure 3. A comparison of N_{HI} with M_{H_2}/M_{HI} for the extra-disk positions in Tables 5 and 6 with both HI and CO data. For comparison purposes, the standard Galactic N_{H_2}/I_{CO} ratio is used to calculate the molecular gas masses. As discussed in the text, this ratio may not hold in all cases. The unlabeled points near $M_{H_2}/M_{HI} \sim 0.8 - 0.9$ and $N_{HI} \sim 10^{20} \text{ cm}^{-2}$ are the data for the Arp 143 tail, the two positions in the Arp 144 tail, the NGC 2782 western tail, and the NGC 4410 tail (see Tables 5 and 6).

Figure 4. The M_{H_2}/M_{HI} ratio plotted against the $L_{H\alpha}/M_{H_2}$ ratio for the extra-disk sources with HI, CO, and $H\alpha$ measurements available.

TABLE 1
INTERACTING GALAXY SYSTEMS IN SAMPLE^a

System Name	Galaxies/Tails/Bridges	Optical and HI Morphology
Arp 144	NGC 7828	Ring Galaxy ^b
	NGC 7829	Spheroidal ^b
	HI Plume ^c	No Detected Optical Counterpart ^c
NGC 2814/2820 Group	NGC 2814	Sb
	NGC 2820	SB(s)c pec
	MK 208	I0 Pec; near NGC 2814/20 Bridge
	NGC 2814/20 Bridge	Visible in Radio Continuum ^d
NGC 3395/6	NGC 3395	SAB(rs)cd pec
	NGC 3396	IBm pec
	NGC 3395/6 Bridge	Visible in Radio Continuum ^e
Arp 105	NGC 3561A	SA(r)a Pec
	NGC 3561B	S0 Pec
	NGC 3561 Irregular ^f	Connected by Stellar Bridge to NGC 3561A
	NGC 3561 Compact Dwarf ^f	Immediately South of NGC 3561B
Leo Triplet	NGC 3627	SAB(s)b
	NGC 3623	SAB(rs)a
	NGC 3628	Sb Pec
	NGC 3628 Tail	Visible in Optical and HI Maps ^g
I Zw 192 System	I Zw 192	Ring or Loop-like Optical Structure ^h
	I Zw 192 Companion	Compact Galaxy Connected by Bridge ^h
	I Zw 192 Plume	Plume Extending from Companion ^h

TABLE 1 (Continued)
INTERACTING GALAXY SYSTEMS IN SAMPLE^a

System Name	Galaxies/Tails/Bridges	Optical and HI Morphology
Stephan’s Quintet	NGC 7317	E4
	NGC 7318A	E2 pec
	NGC 7318B	SB(s)bc pec
	NGC 7319	SB(s)bc pec
	NGC 7320	SA(s)d; Foreground Galaxy
	NGC 7320C	(R)SAB(s)0/a
	Star Formation Region A	North of NGC 7318B, Near Optical Tails
Taffy Galaxies	UGC 12914	(R)S(r)cd pec
	UGC 12915	Sc
	UGC 12914/5 Bridge	Visible in Radio Continuum and HI ⁱ
Arp 284	NGC 7714	SB(s)b pec
	NGC 7715	Im pec
	NGC 7714/5 Bridge	HI Offset from Optical Bridge ^j
	NGC 7714 Loop	Visible in Optical and HI Maps ^j
	NGC 7715 Tail	Visible in Optical and HI Maps ^j

^aAll information from the NASA Extragalactic Database (NED), unless otherwise noted. ^bFreeman & de Vaucouleurs 1974. ^cHigdon 1988; Figure 1a. ^dBosma et al. 1980; van der Hulst & Hummel 1985. ^eHuang et al. 1994. ^fDuc & Mirabel 1994. ^gKormendy & Bahcall 1974; Rots 1978; Haynes, Giovanelli, & Roberts 1979. ^hSmith 1989; Figure 1f. ⁱCondon et al. 1993. ^jSmith et al. 1997.

TABLE 2
CO (1-0) OBSERVATIONS

Name	Position Observed						Central Velocity
	R.A. (1950)			Dec. (1950)			(km s ⁻¹)
NGC 7828	0	3	53.7	−13	41	40.0	5770
Arp 144 Tail #1	0	4	4.2	−13	43	57.7	5700
Arp 144 Tail #2	0	4	10.2	−13	45	16.0	5700
NGC 2814	9	17	9.2	64	27	50.0	1634
NGC 2814/20 Bridge	9	17	15.5	64	27	23.0	1580
MK 208	9	17	26.9	64	27	7.0	1580
NGC 2820	9	17	43.7	64	28	16.0	1580
NGC 2820 NE1	9	17	47.0	64	28	28.9	1580
NGC 2820 NE2	9	17	50.3	64	28	41.8	1580
NGC 2820 NE3	9	17	53.6	64	28	54.6	1580
NGC 2820 NE4	9	17	56.9	64	29	7.5	1580
NGC 3395	10	47	2.7	33	14	44.0	1620
NGC 3395/6 Bridge	10	47	6.0	33	15	5.8	1620
NGC 3396	10	47	8.9	33	15	18.0	1620
NGC 3561A	11	8	31.3	28	59	0.9	8810
NGC 3561 Irregular	11	8	31.4	29	2	12.1	8670
NGC 3561B	11	8	31.5	28	58	5.5	8500, 8700
NGC 3628	11	17	40.3	13	51	46.0	880
NGC 3628 Tail #1	11	19	46.3	13	54	57.0	880
NGC 3628 Tail #2	11	20	38.0	13	59	0.0	880

TABLE 2 (Continued)
CO (1-0) OBSERVATIONS

Name	Position Observed							Central Velocity (km s ⁻¹)
	R.A. (1950)			Dec. (1950)				
I Zw 192	17	39	14.4	38	45	21.0	12100, 12300	
I Zw 192 Companion	17	39	18.4	38	46	12.0	12300	
I Zw 192 Plume	17	39	19.6	38	46	37.0	12300	
NGC 7318A	22	33	39.3	33	42	22.2	6630	
NGC 7318B	22	33	40.9	33	42	24.1	5774	
Stephan's Quintet A	22	33	41.2	33	43	21.5	5774, 6630	
NGC 7319	22	33	46.0	33	42	59.4	6764	
NGC 7714 West	23	33	38.9	1	52	42.0	2800	
NGC 7714 South	23	33	40.6	1	52	17.0	2800	
NGC 7714 Center	23	33	40.6	1	52	42.0	2800	
NGC 7714 North	23	33	40.6	1	53	7.0	2800	
NGC 7714 Loop	23	33	40.6	1	53	32.0	2800	
NGC 7714 East	23	33	42.3	1	52	42.0	2800	
NGC 7714/5 Bridge	23	33	44.9	1	52	50.0	2800	
NGC 7715 Center	23	33	48.3	1	52	48.0	2800	
NGC 7715 Tail	23	33	51.1	1	53	12.0	2800	
UGC 12914 SW2	23	59	0.4	23	11	44.0	4371	
UGC 12914 NW2	23	59	1.6	23	13	17.0	4371	
UGC 12914 SW1	23	59	2.4	23	12	3.0	4371	
UGC 12914 NW1	23	59	3.0	23	12	50.0	4371	

TABLE 2 (Continued)
CO (1-0) OBSERVATIONS

Name	Position Observed						Central Velocity
	R.A. (1950)			Dec. (1950)			(km s ⁻¹)
UGC 12914 Center	23	59	4.4	23	12	22.0	4371
UGC 12914 SE1	23	59	5.8	23	11	54.0	4371
UGC 12914 Bridge	23	59	6.4	23	12	41.0	4371
UGC 12914 SE2	23	59	7.2	23	11	26.8	4371
UGC 12915 Center	23	59	8.3	23	13	00.0	4371

TABLE 3
CO (1-0) RESULTS

Name	T_R^* (rms) ^a	I_{CO}^b	Line Velocity	ΔV^c
	(mK)	(K km s ⁻¹)	(km s ⁻¹)	(km s ⁻¹)
NGC 7828 ^d	2.5	1.16 ± 0.13	5620	625
Arp 144 Tail #1	2.5	$\leq 0.13^e$		
Arp 144 Tail #2 ^d	2.4	$\leq 0.13^e$		
NGC 2814	2.0	0.27 ± 0.07	1710	260
NGC 2814/20 Bridge	3.6	$\leq 0.59^f$		
MK 208	3.0	$\leq 0.49^f$		
NGC 2820	4.3	1.39 ± 0.23	1620	570
NGC 2820 NE1	5.1	$\leq 0.83^f$		
NGC 2820 NE2	5.3	$\leq 0.87^f$		
NGC 2820 NE3	7.4	$\leq 1.21^f$		
NGC 2820 NE4	5.5	$\leq 0.90^f$		
NGC 3395	4.4	1.19 ± 0.17	1600	360
NGC 3395/6 Bridge	3.6	0.92 ± 0.18	1660	420
NGC 3396	5.1	0.55 ± 0.14	1700	150
NGC 3561A	4.0	2.12 ± 0.21	8750	550
NGC 3561 Irregular	2.3	$\leq 0.20^g$		
NGC 3561B	3.8, 4.3, 2.8	$\leq 0.19^g$		
NGC 3628	4.8	29.58 ± 0.25	860	400
NGC 3628 Tail #1	2.3	$\leq 0.13^h$		
NGC 3628 Tail #2	2.2	$\leq 0.13^h$		

TABLE 3
CO (1-0) RESULTS

Name	T_R^* (rms) ^a (mK)	I_{CO} ^b (K km s ⁻¹)	Line Velocity (km s ⁻¹)	ΔV ^c (km s ⁻¹)
I Zw 192	2.5, 1.9, 1.3	1.41 ± 0.07	12130	600
I Zw 192 Companion	2.0	$\leq 0.34^i$		
I Zw 192 Plume	3.1	$\leq 0.52^i$		
NGC 7318A	12.7	$\leq 2.13^j$		
NGC 7318B	2.3	0.47 ± 0.12	6000	400
Stephan's Quintet A	1.8, 1.7, 1.0	$0.296 \pm 0.059, 0.286 \pm 0.048$	6000, 6700	140, 180
NGC 7319	2.7	1.90 ± 0.15	6730	470
NGC 7714 West	4.1	0.65 ± 0.14	2800	230
NGC 7714 South	3.0	0.50 ± 0.14	2780	390
NGC 7714 Center	2.6	1.43 ± 0.08	2800	200
NGC 7714 North	3.9	0.84 ± 0.13	2800	220
NGC 7714 Loop	4.4	$\leq 0.33^k$		
NGC 7714 East	3.1	1.21 ± 0.11	2850	250
NGC 7714/5 Bridge	2.4	$\leq 0.15^k$		
NGC 7715 Center	2.7	$\leq 0.21^k$		
NGC 7715 Tail	3.1	$\leq 0.16^k$		
UGC 12914 SW2	11.4	$\leq 1.91^l$		
UGC 12914 NW2	13.5	$\leq 2.26^l$		
UGC 12914 SW1	8.2	$\leq 1.37^l$		
UGC 12914 NW1	13.1	4.89 ± 0.75	4200	620

TABLE 3
CO (1-0) RESULTS

Name	T_R^* (rms) ^a (mK)	I_{CO} ^b (K km s ⁻¹)	Line Velocity (km s ⁻¹)	ΔV ^c (km s ⁻¹)
UGC 12914 Center	6.1	6.50 ± 0.29	4330	600
UGC 12914 SE1	8.2	4.10 ± 0.33	4550	310
UGC 12914 Bridge	8.1	12.63 ± 0.53	4500	830
UGC 12914 SE2	9.7	$\leq 1.63^l$		
UGC 12915 Center	8.7	12.07 ± 0.43	4460	730

^aAs noted in Table 2 and in the text, at three positions two sets of observations were made at two different central velocities, in order to increase the observed bandpass. In these cases, the rms values listed correspond to the noise levels for the lower velocity spectrum, the higher velocity spectrum, and the combined overlap region, respectively. Note that for Stephan’s Quintet A, two lines were detected, at two different velocities. ^bStatistical uncertainties only. ^cFull width zero maximum (FWZM) line widths. ^dCombined with data from Smith & Higdon 1994. ^eUsing $\Delta v = 60$ km s⁻¹, from the HI data of Higdon 1988. ^fUsing the CO line width of NGC 2820 of 570 km s⁻¹. ^gUsing the HI line widths of 98 km s⁻¹ for NGC 3561B and 161 km s⁻¹ for the NGC 3561 dwarf, from Duc et al. 1997. ^hUsing the HI line width of 70 km s⁻¹ from Rots 1978. ⁱUsing the CO line width of I Zw 192, 600 km s⁻¹. ^jAssuming a line width of ≤ 600 km s⁻¹. ^kUsing the HI line widths of 80 km s⁻¹ for the bridge, 130 km s⁻¹ for NGC 7715, 60 km s⁻¹ for the eastern tail of NGC 7715, and 120 km s⁻¹ for the northern loop. These widths were obtained from the combined HI dataset of Smith & Wallin 1992 and Smith et al. 1997. ^lUsing the CO line width of UGC 12914, 600 km s⁻¹.

TABLE 4
PARAMETERS OF THE MAIN DISKS OF THE SAMPLE GALAXIES

Name	$M(H_2)^a$ (M_\odot)
NGC 7828	3.0×10^9
NGC 2820	3.1×10^8
NGC 2814	6.0×10^7
NGC 3395	2.4×10^8
NGC 3396	1.1×10^8
NGC 3561A	1.3×10^{10}
NGC 3561B	$\leq 1.2 \times 10^9$
NGC 3628	1.6×10^9
I Zw 192	1.7×10^{10}
I Zw 192 Companion	$\leq 4.1 \times 10^9$
NGC 7318A	$\leq 7.6 \times 10^9$
NGC 7318B	1.7×10^9
NGC 7319	6.7×10^9
NGC 7714	2.2×10^9
NGC 7715	$\leq 1.3 \times 10^8$
UGC 12914	1.7×10^{10}
UGC 12915	1.9×10^{10}

^aCalculated assuming the standard Galactic N_{H_2}/I_{CO} ratio ($M_{H_2} = 1.1 \times 10^4 D^2 \int S_V dV$, where D is the distance in Mpc; Bloemen et al. 1986), $H_o = 75 \text{ km s}^{-1} \text{ Mpc}^{-1}$, and assuming 34 Jy/K for the 12m telescope and the source fills the beam ($\eta_c = 0.82$). For the two sources with more than one position detected in the disk, the data were fit to a

Gaussian distribution as in Young et al. 1995.

TABLE 5
PARAMETERS OF THE EXTRA-DISK REGIONS^a

Name	Θ (kpc)	$M_{H_2}^b$ ($10^8 M_\odot$)	$N_{H_2}^b$ (cm^{-2})	N_{HI} (cm^{-2})	$\frac{M_{H_2}}{M_{HI}}$	$L_{H\alpha}^c$ (erg s^{-1})	$\frac{L_{H\alpha}}{M_{H_2}}$ ($\frac{L_\odot}{M_\odot}$)
Arp 144 Tail #1	21	≤ 3.3	$\leq 4.4 \times 10^{19}$	9.7×10^{19}	≤ 0.91		
Arp 144 Tail #2	21	≤ 3.3	$\leq 4.4 \times 10^{19}$	1.1×10^{20}	≤ 0.81		
NGC 2814/20 Bridge	5.6	≤ 1.1	$\leq 2.0 \times 10^{20}$				
MK 208	5.6	≤ 1.1	$\leq 1.7 \times 10^{20}$				
NGC 3395 Bridge ^d	5.9	≤ 1.9	$\leq 3.1 \times 10^{20}$				
NGC 3561 Irregular ^e	31	≤ 12	$\leq 6.8 \times 10^{19}$	7×10^{20}	≤ 0.20	$\geq 8 \times 10^{38}$	≥ 0.00018
NGC 3628 Tail #1	3.2	≤ 0.072	$\leq 4.4 \times 10^{19}$				
NGC 3628 Tail #2	3.2	≤ 0.072	$\leq 4.4 \times 10^{19}$				
I Zw 192 Plume	43	≤ 62	$\leq 1.8 \times 10^{20}$				
SQ A ^f , 6000 km s^{-1}	24	11	1.0×10^{20}	2.5×10^{20}	0.80	1.2×10^{41}	0.016
SQ A ^f , 6700 km s^{-1}	24	10	9.8×10^{19}	2.5×10^{20}	0.78		
NGC 7714 Loop	9.9	≤ 2.1	$\leq 1.1 \times 10^{20}$	9.2×10^{20}	≤ 0.24		
NGC 7714/5 Bridge ^g	9.9	≤ 0.94	$\leq 5.0 \times 10^{19}$	1.6×10^{21}	≤ 0.063	1.8×10^{39}	≥ 0.005
NGC 7715 Tail	9.9	≤ 1.0	$\leq 5.5 \times 10^{19}$	6.5×10^{20}	≤ 0.16		
UGC 12914 Bridge ^d	15	≤ 190	$\leq 4.3 \times 10^{21}$				

^aAll values averaged over the 55'' NRAO 12m beam. ^bCalculated assuming the standard Galactic N_{H_2}/I_{CO} ratio ($N_{H_2}/I_{CO} = 2.8 \times 10^{20} \text{ cm}^{-2}/(\text{K km s}^{-1})$ and $M_{H_2} = 1.1 \times 10^4 D^2 \int S_V dV$, where D is the distance in Mpc; Bloemen et al. 1986), $H_o = 75 \text{ km s}^{-1} \text{ Mpc}^{-1}$, and assuming 34 Jy/K for the 12m telescope and the source fills the beam ($\eta_c = 0.82$). As noted in the text, these assumptions may not hold for all these sources; they are used for comparison purposes here. ^cNot corrected for extinction. ^dBecause this position is

separated from the main disk of the galaxies by less than half of the FWHM beamwidth, the molecular gas mass is given as an upper limit here. ^eH α luminosity from Duc & Mirabel 1994. This was obtained via spectroscopy with a 1.5'' slit and so is a lower limit. ^fHI values from Shostak et al. 1984. Both velocity components are included in the L_{H α} and L_{H α} /M_{H₂} values given here. ^gDerived from the data presented in Smith et al. 1997.

TABLE 6
PARAMETERS OF ADDITIONAL EXTRA-DISK REGIONS^a

Name	Θ (kpc)	$M_{H_2}^b$ ($10^8 M_\odot$)	$N_{H_2}^b$ (cm^{-2})	N_{HI} (cm^{-2})	$\frac{M_{H_2}}{M_{HI}}$	$L_{H\alpha}^c$ (erg s^{-1})	$\frac{L_{H\alpha}}{M_{H_2}}$ ($\frac{L_\odot}{M_\odot}$)
Arp 143 Tail ^d	14	≤ 2.0	$\leq 5 \times 10^{19}$	1.1×10^{20}	≤ 0.9		
Arp 245 ^e	3.5	1.5	3.6×10^{20}	2.3×10^{21}	0.31	5.2×10^{39}	0.009
M81 CO Clump ^f	0.36	~ 0.01	8×10^{20}	10^{21}	1.6		
NGC 3077 CO Clump ^g	0.36	~ 0.01	8×10^{20}	1.5×10^{21}	1.1		
NGC 2782 East Tail ^h	14 ^d	6	2×10^{20}	6×10^{20}	0.6	4×10^{39}	0.002
NGC 2782 West Tail ^d	14	≤ 1.3	$\leq 8.5 \times 10^{19}$	1.1×10^{20}	≤ 0.9		
NGC 3561 South Tail ⁱ	13	2.3	8×10^{19}	2.2×10^{20}	0.8	$\geq 1.3 \times 10^{40}$	≥ 0.015
NGC 4038/9 Tail ^j	6.1	0.84	1.2×10^{20}	8×10^{20}	0.3	1.7×10^{39}	0.005
NGC 4438 CO Clump ^k	1.8	8.4	2.0×10^{21}	9.2×10^{20}	5	$\leq 1.6 \times 10^{39}$	≤ 0.0005
NGC 4410A+B Tail ^l	26	≤ 8	$\leq 4 \times 10^{19}$	9×10^{19}	≤ 0.9		
NGC 4676 North Tail ^j	23	≤ 6.0	$\leq 5.9 \times 10^{19}$	2.1×10^{20}	≤ 0.6	1.1×10^{40}	≥ 0.01
NGC 7252 North Tail ^d	17	≤ 2.4	$\leq 4.5 \times 10^{19}$	1.8×10^{20}	≤ 0.5		
NGC 7252 South Tail ^d	17	≤ 4.5	$\leq 8.5 \times 10^{19}$	1.4×10^{20}	≤ 1.2		

^aAll values averaged over the 55'' NRAO 12m beam, except where noted. ^bCalculated assuming the standard Galactic N_{H_2}/I_{CO} ratio ($N_{H_2}/I_{CO} = 2.8 \times 10^{20} \text{ cm}^{-2}/(\text{K km s}^{-1})$ and $M_{H_2} = 1.1 \times 10^4 D^2 \int S_V dV$, where D is the distance in Mpc; Bloemen et al. 1986), $H_o = 75 \text{ km s}^{-1} \text{ Mpc}^{-1}$, and assuming 34 Jy/K for the 12m telescope and the source fills the beam ($\eta_c = 0.82$). As noted in the text, these assumptions may not hold for all these sources; they are used for comparison purposes here. ^cNot corrected for extinction. ^dAs tabulated in Smith & Higdon 1994. ^eUsing the data from Braine et al. 2000 and Duc et al. 2000, in a $\sim 23''$ beam. The $H\alpha$ luminosity has been corrected for [N II] using

$\text{H}\alpha/(\text{H}\alpha + [\text{N II}]) \sim 0.7$, as indicated by the spectroscopy in Duc et al. (2000). ^fUsing the data from Brouillet et al. 1992 and Rots & Shane 1975, in a $\sim 23''$ beam. No evidence of star formation at this position has been observed (Henkel et al. 1993). The assumed distance is 3.2 Mpc (Sandage & Tammann 1978; Humphreys & Aaronson 1987). ^gUsing the data from Walter & Heithausen 1999, in a $\sim 23''$ beam. There is no observed star formation at this position (Walter & Heithausen 1999). The HI column density quoted here was estimated from the HI map in Walter & Heithausen 2000. ^hFrom data in Smith et al. 1999. These are averaged over the five detected positions in the tail, covering an area of $\sim 7645 \text{ arcsec}^{-2}$, the equivalent of an $87''$ beam. ⁱUsing the data from Braine et al. 2000, Duc & Mirabel 1994, and Duc et al. 1997, in a $\sim 23''$ beam. The $\text{H}\alpha$ flux was derived from spectroscopy with a $1.5''$ slit, and so is an upper limit. ^jThe CO measurement is a tentative (4σ) detection from Gao et al. 2000; note that this assumes a broader line (175 km s^{-1}) than the upper limit quoted in Smith & Higdon 2000. The HI measurement is estimated from the Hibbard et al. (2000) HI map. The $\text{H}\alpha$ measurement is from Mirabel et al. 1992. ^kAs tabulated in Smith et al. 1999, in a $23''$ beam. ^lUsing the data from Smith 2000.

This figure "bsmith_fig1a.jpg" is available in "jpg" format from:

<http://arxiv.org/ps/astro-ph/0011093v1>

This figure "bsmith_fig1b.jpg" is available in "jpg" format from:

<http://arxiv.org/ps/astro-ph/0011093v1>

This figure "bsmith_fig1c.jpg" is available in "jpg" format from:

<http://arxiv.org/ps/astro-ph/0011093v1>

This figure "bsmith_fig1d.jpg" is available in "jpg" format from:

<http://arxiv.org/ps/astro-ph/0011093v1>

This figure "bsmith_fig1e.jpg" is available in "jpg" format from:

<http://arxiv.org/ps/astro-ph/0011093v1>

This figure "bsmith_fig1f.jpg" is available in "jpg" format from:

<http://arxiv.org/ps/astro-ph/0011093v1>

This figure "bsmith_fig1g.jpg" is available in "jpg" format from:

<http://arxiv.org/ps/astro-ph/0011093v1>

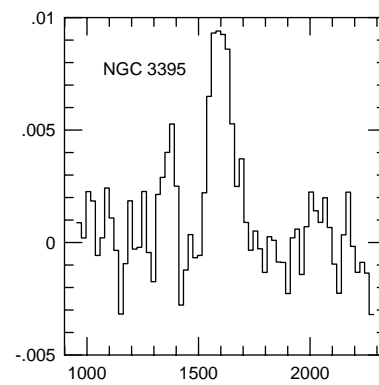
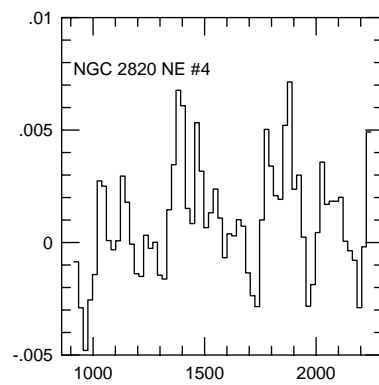
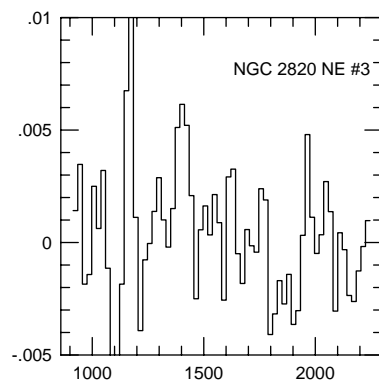
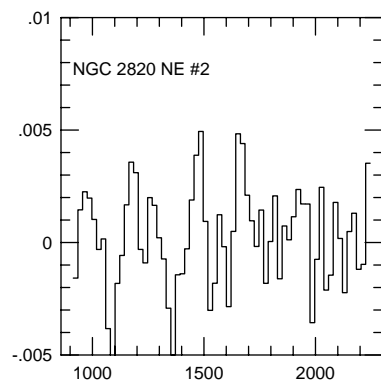
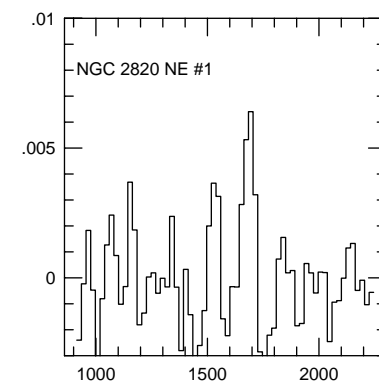
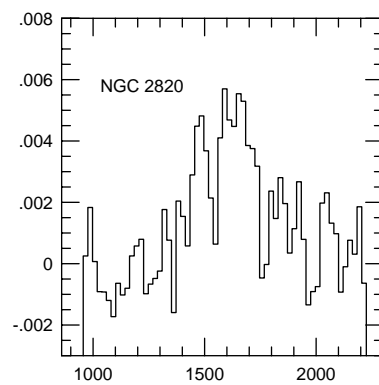
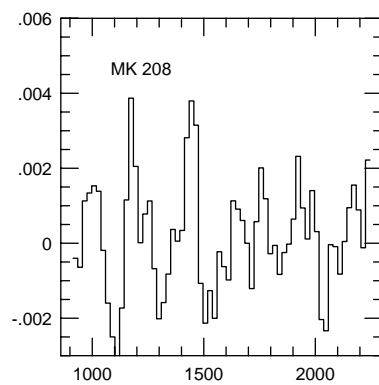
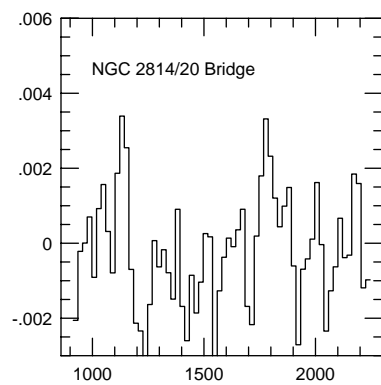
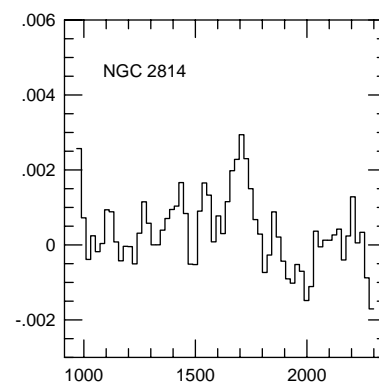
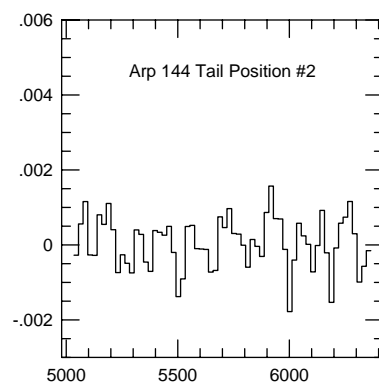
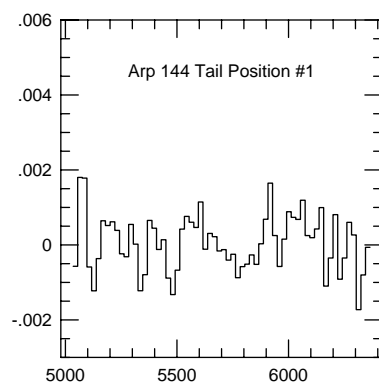
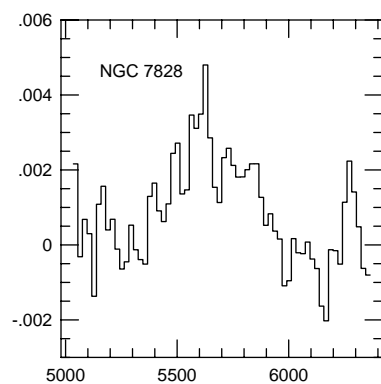
This figure "bsmith_fig1h.jpg" is available in "jpg" format from:

<http://arxiv.org/ps/astro-ph/0011093v1>

This figure "bsmith_fig1i.jpg" is available in "jpg" format from:

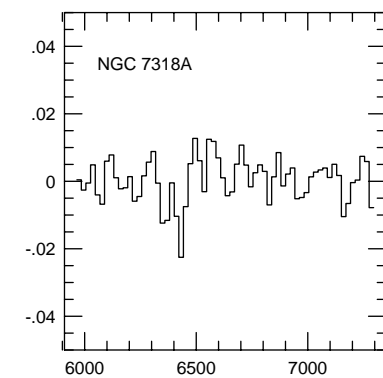
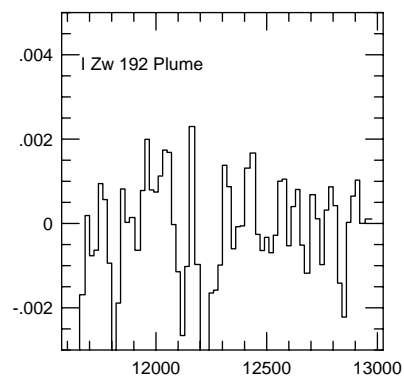
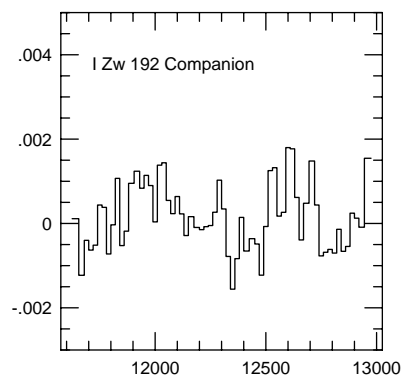
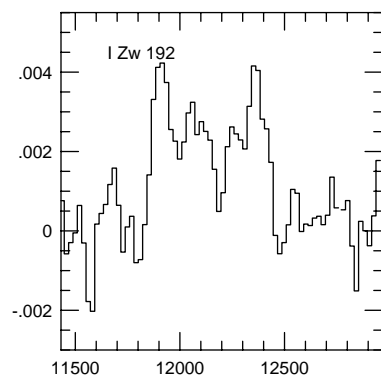
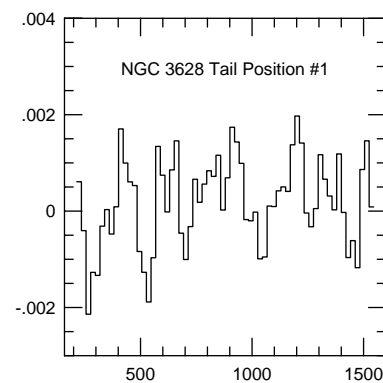
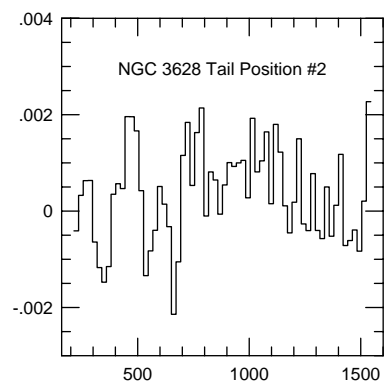
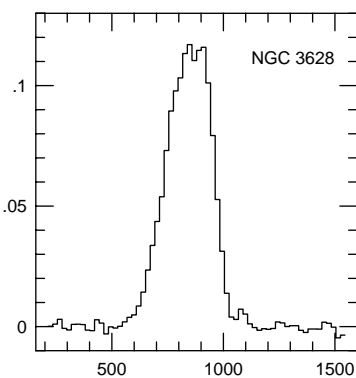
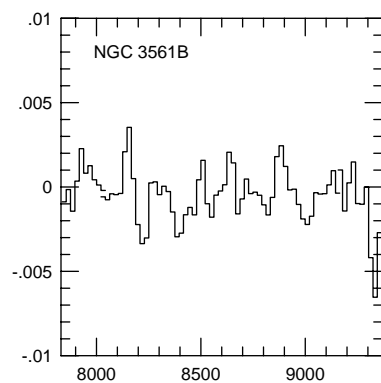
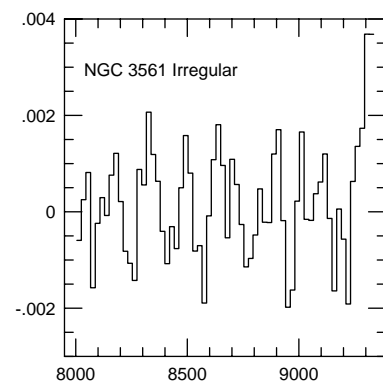
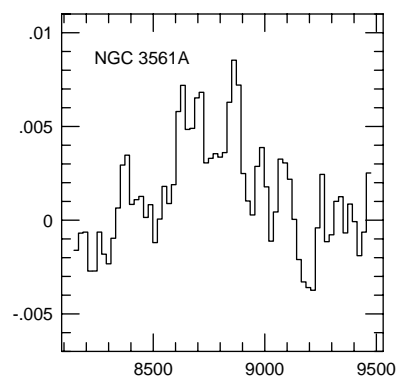
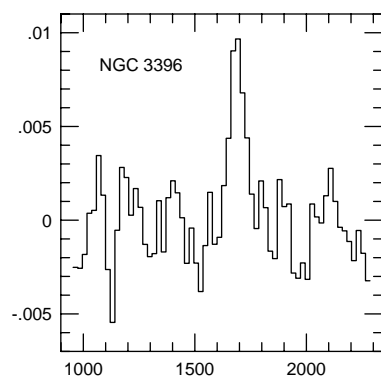
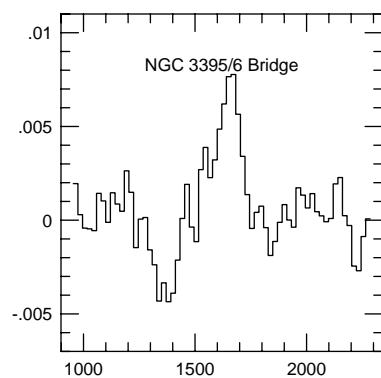
<http://arxiv.org/ps/astro-ph/0011093v1>

T_R^* (K)



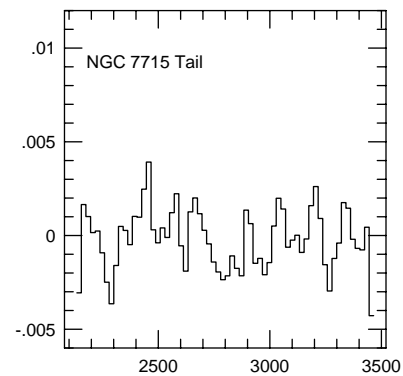
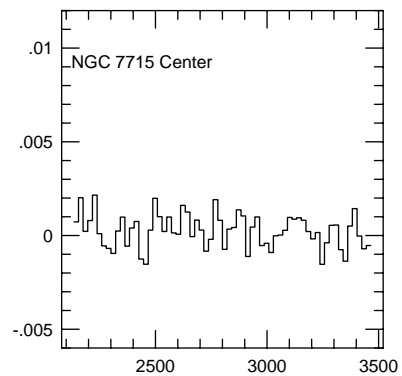
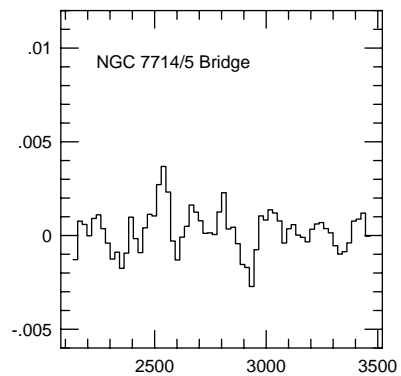
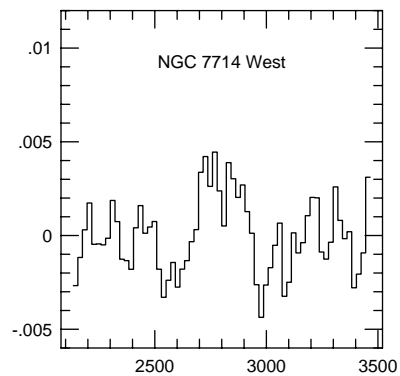
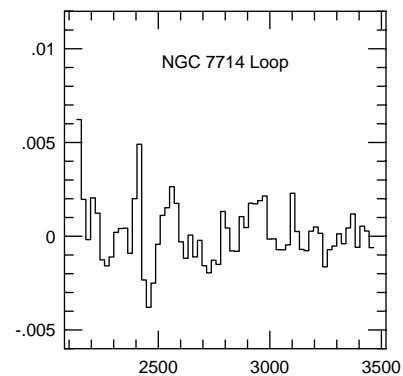
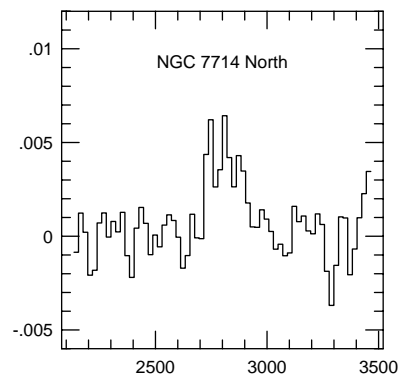
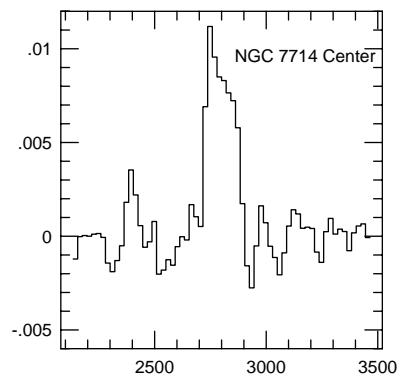
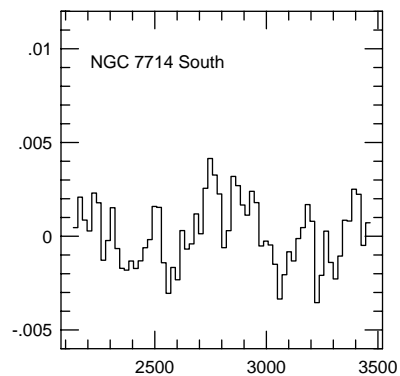
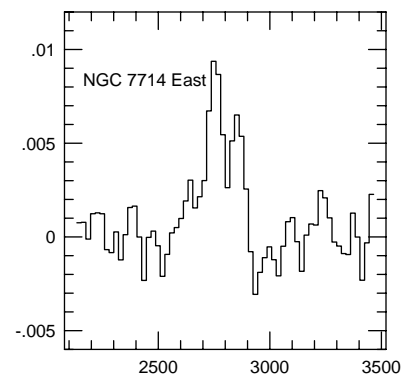
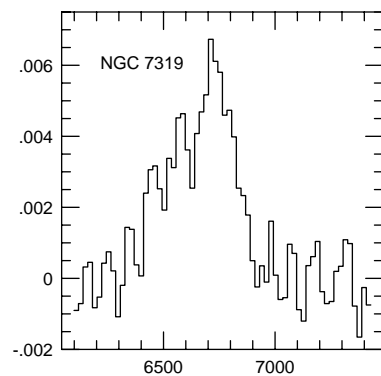
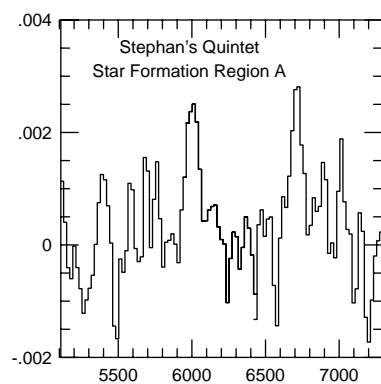
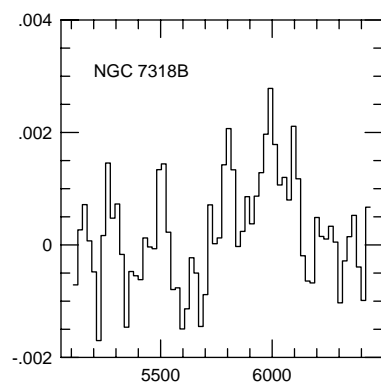
VELOCITY (km/s)

T_R^* (K)



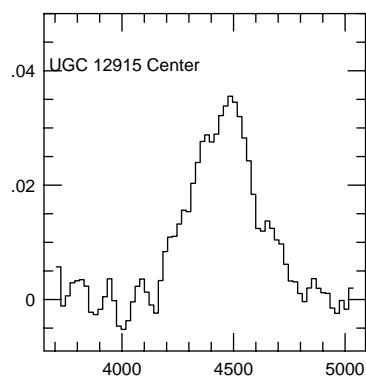
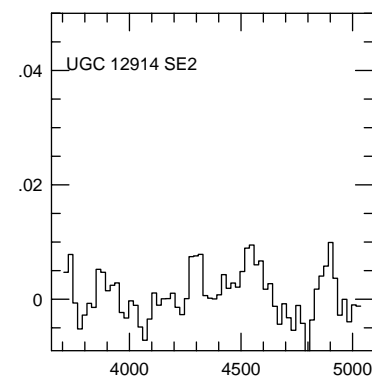
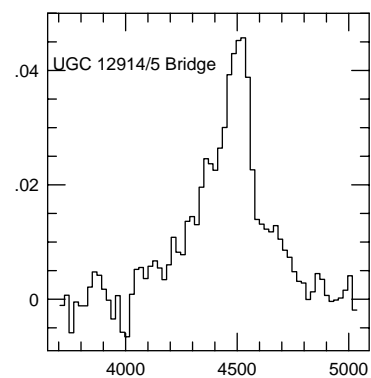
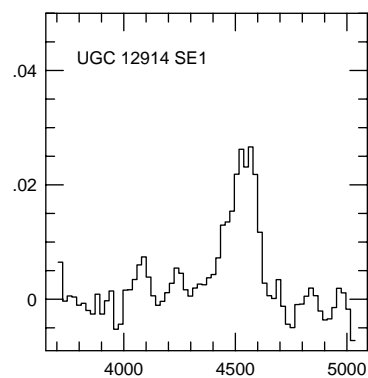
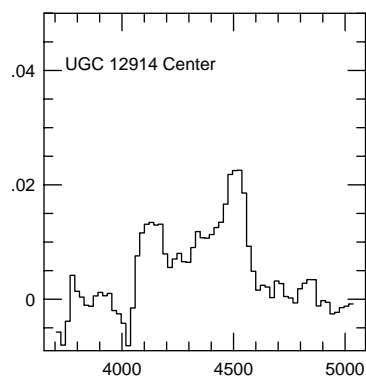
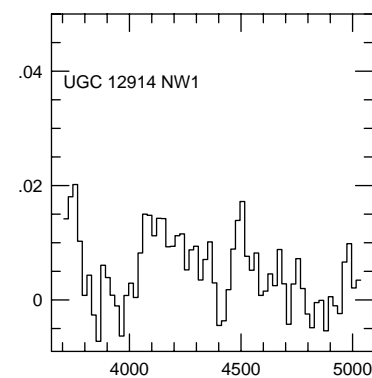
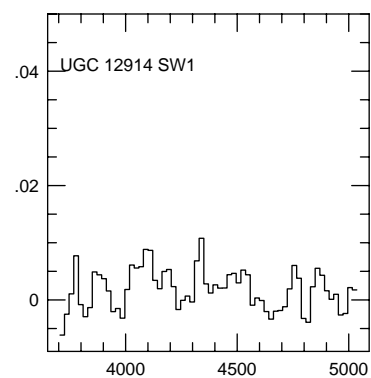
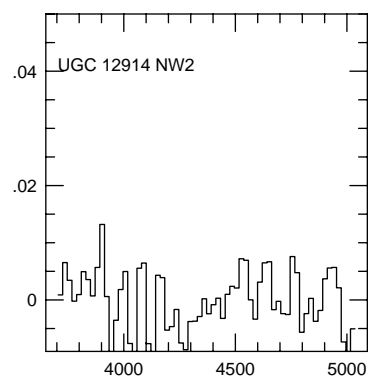
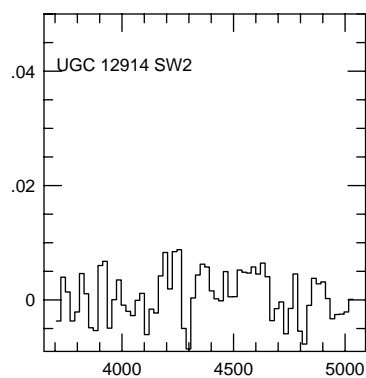
VELOCITY (km/s)

T_R^* (K)



VELOCITY (km/s)

T_R^* (K)



VELOCITY (km/s)

